Wiedemann−Franz Relation and Thermal-Transistor Effect in Suspended Graphene

S. Yiğen and A. R. Champagne*

Department of Physics, Concordia University, Montréal, Québec, H4B 1R6 Canada

S *Supporting Information*

ABSTRACT: We extract experimentally the electronic thermal conductivity, K_e, in suspended graphene that we dope using a back-gate electrode. We make use of two-point dc electron transport at low bias voltages and intermediate temperatures (50−160 K), where the electron and lattice temperatures are decoupled. The thermal conductivity is proportional to the charge conductivity times the temperature, confirming that the Wiedemann−Franz relation is obeyed in suspended graphene. We extract an estimate of the Lorenz coefficient as $1.1-1.7 \times 10^{-8}$ W ΩK^{-2}. K_e shows a transistor effect and can be tuned with the back-gate by more than a factor of 2 as the charge carrier density ranges from ∼0.5 to 1.8×10^{11} cm^{-2}.

KEYWORDS: *Graphene, thermal conductivity, Wiedemann−Franz, thermal transistor, electron−phonon*
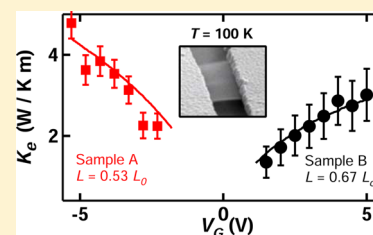
Graphene's electronic thermal conductivity, K_e, describes how easily Dirac charge carriers (electron and hole quasiparticles) can carry energy. In low-disorder graphene at moderate temperatures (<200−300 K), the energy transfer rate between charge carriers and acoustic phonons is extremely slow.[1−6] Thus, K_e impacts how a hot electron cools down, and the efficiency of charge harvesting in graphene optoelectronic devices.[1,2,7] Moreover, understanding and controlling K_e could help develop graphene bolometers capable of detecting single terahertz photons.[4,8] There are theoretical calculations of K_e,[9−11] and recent experimental data near the charge neutrality point (CNP) in clean suspended graphene[6] and in disordered samples at very low temperatures.[4,8] However, a detailed mapping of K_e versus charge density at intermediate temperatures is lacking. Understanding how K_e in clean (suspended) graphene depends on charge density, n, and the electronic temperature, T_e, is crucial for applications. An important fundamental question is whether the Wiedemann−Franz (WF) law, $K_e = \sigma L T_e$ where σ is the charge conductivity and L is the Lorenz number, is obeyed in graphene. In clean graphene at low charge densities (hydrodynamic regime), strong electron−electron interactions could lead to departures from the generalized WF law.[10,11]

We report K_e in monolayer graphene extracted from carefully calibrated dc electron transport measurements following a method we previously discussed.[6] We study a temperature range of T = 50−160 K, where the electron and lattice temperatures are very well decoupled in low-disorder graphene[1−6] over a charge density range of ∼0.5−1.8 × 10^{11}cm^{-2}. We extract data in the hole and electron-doped regimes from two high-mobility suspended devices. The extracted K_e are compared with predictions from the WF law. The agreement between the WF relation and measurements is very good for both devices over the n range studied and T up to 160 K. The value of L is ≈ 0.5−0.7 L_o, where L_o is the Lorenz

factor for metals. We observe a sudden jump in the extracted thermal conductivity above 160 K that is consistent with the onset of strong coupling between electrons and acoustic phonons.[5] Finally, we observe a thermal transistor effect consistent with the WF prediction, where K_e can be tuned by more than a factor of 2 with a back-gate voltage, V_G, ranging up to ±5 V. Throughout the text we use T to designate the lattice (cryostat) temperature, and T_e for the average electron temperature in the suspended devices. At very low bias, $|V_B|$ ≤ 1 mV, $T = T_e$.

Figure 1a,b shows dc two-point resistance data, $R = V_B/I$, versus gate voltage, V_G, which controls the charge density, n_G (upper axis) for Samples A and B, respectively. From the width of the R maximum at low T, we extract a half width at half-maximum, hwhm, of 0.45 and 0.95 V for Samples A and B. These hwhms correspond to an impurity-induced charge density of $n^* \approx 1.5$ and 2.1×10^{10} cm^{-2}. For clarity, the data in Figure 1 is slightly shifted along the V_G axis so that all the maxima (Dirac points) line up at $V_G = 0$ and the shifts in panel a range from −0.3 to −0.45 V at various T and in panel b from 0 to 0.2 V. The insets in Figure 1 show scanning electron microscope (SEM) tilted images of Sample A and a sample identical to Sample B.

We confirmed, using optical contrast and Raman spectroscopy, that both samples are single-layer graphene. Sample A is 650 nm long, 675 nm wide, and suspended 140 ± 10 nm above the substrate (atomic force microscopy measurement) that consists of 100 ± 2 nm of SiO$_2$ (ellipsometry measurement) on degenerately doped Si that is used as a back-gate electrode. Sample B is 400 nm long, 0.97 μm wide, and suspended 227 ± 10 nm above a 74 ± 2 nm SiO$_2$ film on Si. To prepare the
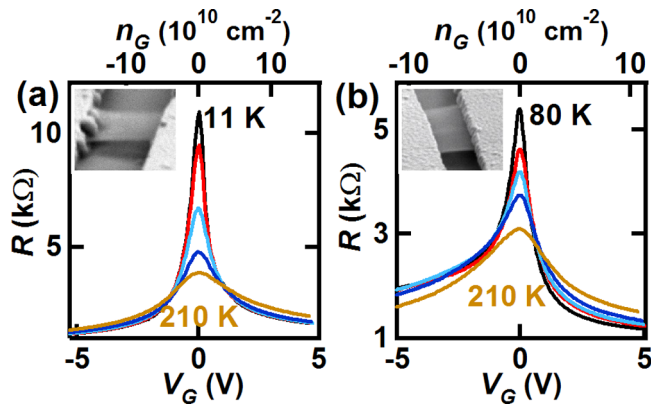
Figure 1. Suspended and annealed graphene devices. (a) R of Sample A versus gate voltage, V_G, at $T_e = T = 11, 50, 100, 150,$ and 210 K and $V_B = 0.5$ mV. (b) $R–V_G$ data for Sample B at $T_e = T = 80, 100, 125, 150,$ and 210 K and $V_B = 5$ mV. The insets show tilted SEM images of the suspended graphene transistors: Sample A (650 nm long) and a device identical to Sample B (400 nm long). For clarity, the data curves in (a) and (b) are slightly shifted along the V_G axis so that all the maxima line up at $V_G = 0$; the shifts in (a) range from -0.3 to -0.45 V and in (b) from 0 to 0.2 V.

samples, we used exfoliated graphene and standard e-beam lithography to define Ti(5 nm)/Au(80 nm) contacts. The samples were suspended with a wet buffered oxide etch such that their only thermal connection was to the gold contacts. We annealed the devices using Joule heating in situ by flowing a large current in the devices[6,12] (see Supporting Information Section 1). Annealing and all subsequent measurements were done under high vacuum, $\leq 10^{-6}$ Torr.

To minimize contact resistance, R_c, the devices were fabricated with large contact areas between the gold electrodes and graphene crystals, ranging from 1.1 to 3 μm^2 per contact. An upper bound for series resistance, R_o, which includes both the contact resistance, R_c, and the resistance from neutral scatterers, can be extracted from the two-point $R–V_G$ curves[13] in Figure 1 (see Supporting Information Section 2). The extracted series resistances for Sample A are $R_{o-h} \approx 477 \pm 53$ and $R_{o-e} \approx 944 \pm 80$ Ω for hole and electron doping, respectively. The difference between R_{o-h} and R_{o-e} is understood as an additional p−n barrier for the electron due to doping from the gold electrodes.[14] For Sample B, we find $R_{o-h} = 1563$ Ω and $R_{o-e} = 812$ Ω. We note that series resistance is smallest for hole doping in Sample A and for electron doping in Sample B. In annealed samples, oxygen desorbs from the gold contacts and changes the work function of the electrodes. This means that graphene under the gold electrodes can be either electron doped or hole doped depending on the thoroughness of the contact annealing.[14−16] To minimize the effect of R_c on our data, we study the lowest resistance side of the Dirac point for each sample. This allows us to study hole transport in Sample A and electron transport in Sample B. Since R_o includes both R_c and the resistance due to neutral scatterers in the channel, we conservatively set $R_c = R_o/2$ with an uncertainty ranging up to $R_{c-max} = R_o$, and down to $R_{c-min} =$ lowest reported resistance for Au/graphene[17] with similar n, which is ∼100 $\Omega \cdot \mu m^2$. Thus, in the following data analysis we use for Samples A and B, $R_{c-A} = 239 \pm {}^{239}_{120}$ and $R_{c-B} = 406 \pm {}^{406}_{281}$. We extract a conservative estimate of the charge carrier mobility in our devices, over the n and T_e range studied, as $\mu = \sigma/(n_{tot}e) \approx 3.5 \times 10^4$ cm^2/V·s, where n_{tot} is the total carrier

density including the gate, impurity, and thermal doping[6,18] (Supporting Information Section 3). On the basis of the reported thermal conductance of Au/Ti/graphene and graphene/SiO$_2$ interfaces,[19] the thermal resistance of the contacts can safely be neglected[20] compared to our K_e data presented below.

Figure 2 summarizes our approach to extract K_e in suspended high-mobility graphene, whose details we previously discussed.[6]
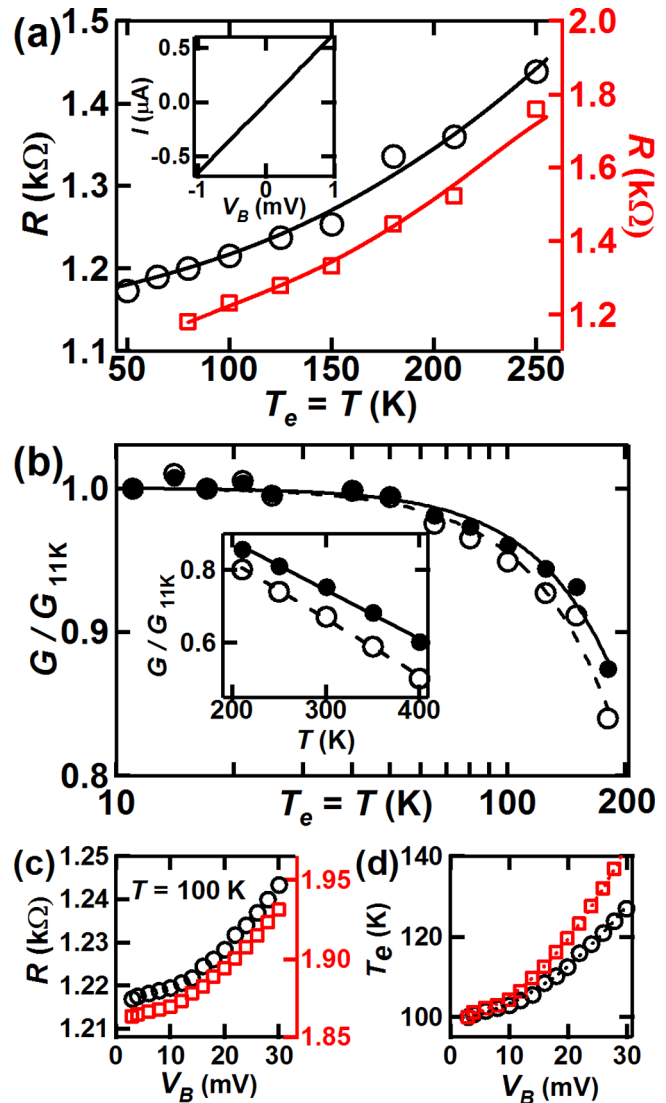
Figure 2. Electron thermometry and electron Joule heating. (a) R versus T_e in Sample A (circles, left axis) and Sample B (squares, right axis), respectively hole ($n_G = -1.8 \times 10^{11}$ cm^{-2}) and electron doped ($n_G = 1.1 \times 10^{11}$ cm^{-2}). The solid lines are numerically interpolated curves used for thermometry. Inset: example of $I−V_B$ data at 100 K for Sample A whose slope is used to extract R, $|V_B| < 1$ mV such that $T_e = T$. (b) Relative conductance G/G_{11K} of Sample A versus $T_e = T$. The solid circles show the raw two-point data and the open circles the data using $R_c = 239$ Ω. The solid and dashed lines are power law fits consistent with charge impurity scattering. Inset: G/G_{11K} of Sample A at high T showing a linear decrease in R consistent with acoustic phonon scattering. (c) R versus V_B data for Sample A at $T = 100$ K, and $n_G = -1.8$ (circles, left axis) and -0.8 (squares, right axis) $\times 10^{11}$ cm^{-2} (i.e., $V_G = -5.3$ and -2.3 V). Joule heating due to V_B raises the flake's average T_e above T. (d) T_e versus V_B in Sample A extracted from (c) using the calibration in (a) and similar curves.

We repeat some of the discussion of our methods because the charge densities studied here are much higher than in ref 6, which leads to several important changes. Figure 2a,b presents how we monitor the charged quasiparticle temperature in our devices by monitoring R, and Figure 2c,d shows how we can controllably heat-up these quasiparticles at a temperature slightly above the contacts' temperature via Joule heating. By combining these two capabilities and using the heat equation, we will later extract K_e versus T and n.

Figure 2a shows the two-point dc R versus cryostat temperature, T, calibration curves for Sample A (circles, left axis), and Sample B (squares, right axis) that are respectively hole-doped with a gate-induced density of $n_G = -1.8 \times 10^{11}$ cm^{-2} and electron-doped with $n_G = 1.1 \times 10^{11}$ cm^{-2}. $R = V_B/I$ is extracted from the slope of the $I - V_B$ data[21] as shown in the inset of Figure 2a. Note that for ± 1 mV bias no Joule heating effect is present and $T_e = T$. The T_e dependence of the data shows a metallic behavior with R increasing with T_e. The interpolated lines in Figure 2a, and similar curves, will be used as secondary thermometry curves to monitor T_e in the devices.

Figure 2b shows the relative conductance $G(T)/G_{11K}$ for Sample A extracted from Figure 2a and similar data. The solid circles show the raw two-point data, and the open circles the data after subtracting $R_c = R_o/2$. The T dependence of $G = 1/R$ in graphene at modest charge density is strongly dependent on the type of charge transport. We fit the data in Figure 2b with a function $G/G_{11K} = 1 - AT^p$ and extract $p = 2.1 \pm 0.2$ for both curves. This T-dependence strongly supports diffusive charge transport dominated by long-range charge impurities, as reported in previous experiments on high-mobility devices[12,22,23] and expected theoretically.[5] The inset of Figure 2b shows that G/G_{11K} of Sample A decreases linearly for $T \geq 200$ K, which suggests a relatively strong acoustic phonon scattering above this temperature, as expected theoretically.[5] Sample B shows a qualitatively identical behavior of its R versus T in Figure 2a, but the absence of low-temperature data proscribes an accurate fit of its dependence. We will focus our measurements on the $T < 200$ K range, where both samples are in the diffusive regime (Supporting Information Section 3) with scattering predominantly due to charged impurities. This scattering is elastic, and its T_e dependence (used for thermometry) comes mostly from the temperature dependence of its screening.[23]

Electron−electron scattering between charge carriers is inelastic. By applying a V_B one can inject high-energy carriers in the suspended device which then thermalize with the carriers in the sample and raise T_e in the suspended graphene relative to the temperature in the gold contacts. Note that when writing T_e, we always refer to the average temperature of charged quasiparticles in our devices. We demonstrate controlled Joule self-heating of the electrons to apply a thermal bias $\Delta T = T_e - T$ between the suspended graphene and the electrodes (cryostat temperature). Figure 2c shows R versus V_B for Sample A at $T = 100$ K and $n_G = -1.8 \times 10^{11}$ (circles, left axis) and -0.8×10^{11} cm^{-2} (squares, right axis). Sample B data is shown in Supporting Information Section 4. R increases monotonically with increasing V_B at all T. We restrict our measurements to $V_B \leq 27$ meV. We have previously argued[6] that in our high-mobility devices under such low V_B and in the T range we study the change in R is caused by Joule heating of the charge carriers.[3,6] Using the curves, R versus T_e and R versus V_B, we extract T_e versus V_B as shown for Sample A in Figure 2d. We fit a power law (dashed lines) $T_e = 100 + BV_B^x$,

and find $x = 1.93 \pm 0.04$ for both data sets, as expected for Joule heating where $T_e \propto V_B^2$. Figure 3d and Supporting
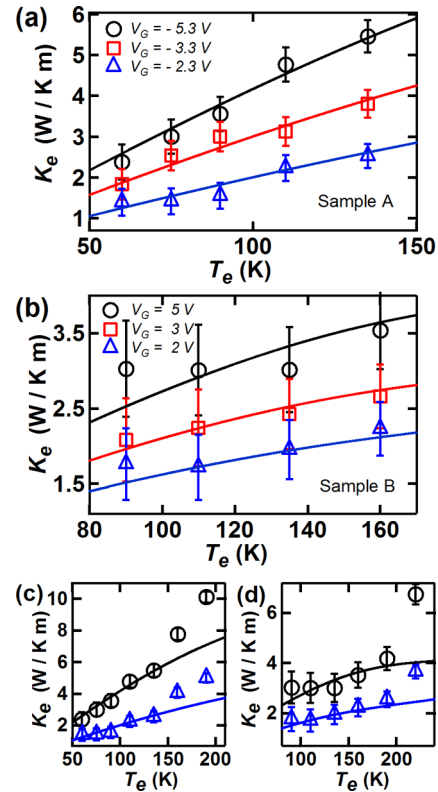
Figure 3. WF law. (a) The electronic thermal conductivity, K_e, of Sample A in the hole-doped regime versus T_e for $\Delta T = T_e - T = 10$ K. The circle, square, and triangle data show K_e at $V_G = -5.3$, -3.3, and -2.3 V, respectively, corresponding to $n_{tot, T=0} \approx -1.8, -1.1, -0.8 \times 10^{11}$ cm^{-2}. The solid lines are given by the WF relation $K_{WF} = L\sigma T_e$ with $L = 0.45, 0.53$, and $0.55 \times L_o$, respectively. (b) K_e versus T_e for $\Delta T = 10$ K for Sample B in the electron-doped regime. The circle, square, and triangle data show K_e at $V_G = 5, 3$, and 2 V corresponding to $n_{tot, T=0} \approx 1.1, 0.7, 0.5 \times 10^{11}$ cm^{-2}. The solid lines are the K_{WF} with $L = 0.66, 0.68, 0.7 \times L_o$. (c,d) The same data as in (a) and (b) up to higher T_e where the apparent departure between the data and WF prediction is understood as the onset of electron−phonon coupling.

Information Figure S3b show that the accuracy with which T_e can be extracted is much better than 1 K. The smooth dependence of T_e on V_B at all T is consistent with electrons having a well-defined temperature as predicted by calculations of the $e−e$ collision length[24] (see Supporting Information of ref 6) and confirmed by the K_e data shown below.

We use a 1-d heat equation[6] to extract K_e in our devices, and find $K_e = (Ql^2)/(12\Delta T)$, where $\Delta T = T_e - T$, $Q = RI^2/Wlh$ is the Joule heating power per unit volume, W is the width, l is the length, $h = 0.335$ nm is the thickness, and T_e is the electronic temperature averaged over l. In Figure 3a,b, we plot K_e versus T_e for Samples A and B for $\Delta T = 10$ K, where the circle, square, and triangle data show K_e at $n_{tot, T=0} \approx -1.8$, $-1.1, -0.8 \times 10^{11}$ cm^{-2} for Sample A, and $n_{tot, T=0} \approx 1.1, 0.7$, 0.5×10^{11} cm^{-2} for Sample B. The quantity $n_{tot, T=0}$ refers to the total charge density induced by V_G and charged impurities (Supporting Information Section 3). We clearly observe that K_e increases with both n and T_e in both samples. For instance, K_e ranges from roughly 1 W/K.m at 60 K and $n = -8 \times 10^{10}$ cm^{-2} to 5 W/K.m at 135 K and $n = -1.8 \times 10^{11}$ cm^{-2} for Sample A.

Error bars representing the uncertainty on the extracted K_e are shown in Figure 3 (Supporting Information Section 5). We confirmed that the V_B needed to create ΔT did not dope significantly the samples or affect the measured K_e.[25] The thermoelectric voltages in our devices are negligible compared to V_B.[26,27]

We test the WF law in our samples, which have a mobility of $\mu \approx 3.5 \times 10^4$ cm^2/V·s, as a function of T_e and n. While the Lorenz number in most metals is close to $L_o = 2.44 \times 10^{-8}$ $W\Omega K^{-2}$, it is well-known that its value can be reduced in semiconductors at low charge density.[28,29] The solid lines in Figure 3 show K_{e-WF} given by the WF law using the measured σ and extracted T_e (Figure 2) with L used as the single fitting parameter. The WF relation holds for both Samples at all T_e between 50 and 160 K, and densities $n_h = -1.8$ to -0.8×10^{11} cm^{-2} and $n_e = 0.5$ to 1.1×10^{11} cm^{-2}. For Sample A, $L = 0.45$, 0.53, and $0.55 \times L_o$, and for Sample B $L = 0.66$, 0.68, $0.7 \times L_o$ (triangle, square, and circle data, respectively). The main uncertainty on L comes from the uncertainty on R_c and corresponds to $\pm {}^{0.1}_{0.2} L_o$ for Sample A, and $\pm 0.4 L_o$ for Sample B. We note that the qualitative temperature and density dependence of the data in Figure 3, and the agreement with the WF law, is preserved even if we use either the maximum $R_c = R_o$ or minimum $R_c = 120 \, \Omega$ (Supporting Information Section 6). The increase in L as n increases is consistent with previous studies in semiconductors where the value of L tends toward L_o at higher carrier density.[29]

Electron to acoustic phonon coupling is very weak in clean graphene at moderate doping and temperature ($<200-300$ K)[1-3,5,6] but increases at higher n and T. In the context of our experiment, if the thermal energy conductance between electrons and phonons G_{e-p} is non-negligeable compared to the electronic thermal conductance G_e, the heat conductivity we extract is a mixture of K_e and K_{e-p} in parallel. As can be seen in Figure 3c,d, above ≈ 160 K the extracted K no longer agrees with the WF prediction (solid line), indicating that we cannot isolate K_e for $T_e > 160$ K. Previously we found that we could extract K_e up to 300 K in samples whose n was very close to the CNP,[6] suggesting that e−p coupling is weaker at lower n as expected theoretically.[5] In Figure 3c,d, the departure between the K data and WF prediction starts around 150 K for Samples A and 200 K for Sample B. The different T ranges over which K_e dominates in the two devices comes from the ratio G_e/G_{e-ph} $= W/(Wl) = 1/l$ which is 60% larger for Sample B than Sample A.

Figure 4 shows the extracted K_e versus V_G at $T_e = T + \Delta T = 100 + 10$ K for Sample A (B) as solid red squares (black circles). For reference only, we also show two data points (open gray symbols) close to $V_G \approx 0$ that are taken from ref 6 for the same samples. We cannot extract K_e at intermediate n, that is, when 0.3 V $\leq |V_G| \leq 1.5$ V. This is because while R smoothly increases with T_e in the metal-like regime (Figure 2a), $|V_G| \geq 1.5$ V, and smoothly decrease in the insulator-like regime,[6] $|V_G| \leq 0.3$ V, the R versus T_e behavior does not act as a good thermometer at intermediate densities. We also note that the WF relation we discuss in this work, $K_e = \sigma L T_e$, only applies in the degenerately doped regime where the Fermi energy $\mu \gg k_B T_e$, and we focus our discussion on this regime. The solid symbol data in Figure 4 show that K_e is tuned by the charge carrier density in the samples. The solid lines are the WF values K_{e-WF} calculated using the measured σ, $T_e = 110$ K, and setting $L = 0.53$ and $0.67 \, L_o$ for Samples A and B. The agreement between the WF law and data in the doped regime is excellent.
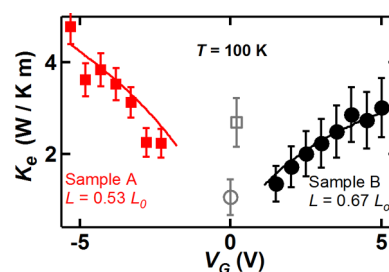
Figure 4. Electronic thermal conductivity transistor effect. K_e versus V_G data for Samples A (solid squares, $n < 0$) and B (solid circles, $n > 0$), for $T = 100$ K and $\Delta T = 10$ K. $V_G \approx 0$ data (open symbols, $\Delta T = 5$ K) are from ref 6. The solid lines show K_{WF} predicted by the Wiedemann−Franz relation using a Lorenz number of $L = 0.53 \, L_o$ and $0.67 \, L_o$ for A and B, respectively.

Even using a modest V_G range, K_e could be tuned by a factor of ≥ 2 in Figure 4. This is a very strong thermal-transistor effect (with the caveat that $K_p \gg K_e$[30,31]). This could have applications in optoelectronics. A larger K_e means that when a charge carrier is excited by a photon, it can travel a larger distance and excite additional carriers before it thermalizes with the lattice. Thus, more of the photon energy is harvested as electrical current.[7] Additionally, a tunable K_e implies a tunable C_e which could be used to optimize bolometric applications of graphene.[4,8]

In summary, we fabricated high-quality suspended graphene devices. We used a self-thermometry and self-heating method[6] to extract the electronic thermal conductivity in doped graphene. We report for the first time K_e in suspended graphene over a broad range of T and n. The data presented clearly demonstrates that $K_e \propto \sigma T$, which confirms that the Wiedemann−Franz law holds in high-mobility ($\mu \approx 3.5 \times 10^4$ cm^2/V·s) suspended graphene over our accessible temperature range, 50−160 K. This temperature range is limited at high-temperature by a turning on of the electron−phonon coupling, which prevents us from isolating K_e at higher T. The clear onsets of the electron−phonon coupling (Figure 2b, and 3c,d) between 150−200K is consistent with theoretical calculations.[5] We studied charge densities of holes and electrons ranging up to 1.8×10^{11} cm^{-2} and found Lorenz numbers $L \approx 0.5-0.7 \, L_o$, where L_o is the standard Lorenz number for metals. The quality of the agreement between the data and the WF relation in Figures 3 and 4 is not affected by the uncertainty on the extracted Lorenz numbers (Supporting Information Section 6). Finally, we demonstrated a strong thermal-transistor effect where we could tune K_e by more than a factor of 2 by applying only a few volts to a gate electrode.

In the future, these measurements could be extended to even cleaner devices at lower densities to study possible corrections to the generalized WF relation due to strong electron−electron interactions.[10,11] The demonstrated density control of K_e could be useful to make energy harvesting optoelectronic devices[1,2,7] and sensitive bolometers.[4,8]

■ ASSOCIATED CONTENT

Ⓢ Supporting Information

We include data on and discussion of the sample annealing, contact resistance, mean-free path of carriers, Joule self-heating, error analysis, and the effect of contact resistance on the extracted Lorenz numbers. This material is available free of charge via the Internet at http://pubs.acs.org.

■ AUTHOR INFORMATION

Corresponding Author
*E-mail: a.champagne@concordia.ca.

Notes

The authors declare no competing financial interest.

■ ACKNOWLEDGMENTS

■ REFERENCES

(1) Gabor, N. M.; Song, J. C. W.; Ma, Q.; Nair, N. L.; Taychatanapat, T.; Watanabe, K.; Taniguchi, T.; Levitov, L. S.; Jarillo-Herrero, P. *Science* **2011**, *334*, 648.

(2) Song, J. C. W.; Rudner, M. S.; Marcus, C. M.; Levitov, L. S. *Nano Lett.* **2011**, *11*, 4688.

(3) Viljas, J. K.; Fay, A.; Wiesner, M.; Hakonen, P. J. *Phys. Rev. B* **2011**, *83*, 205421.

(4) Fong, K. C.; Schwab, K. C. *Phys. Rev. X* **2012**, *2*, 031006.

(5) Das Sarma, S.; Hwang, E. H. *Phys. Rev. B* **2013**, *87*, 035415.

(6) Yigen, S.; Tayari, V.; Island, J. O.; Porter, J. M.; Champagne, A. R. *Phys. Rev. B* **2013**, *87*, 241411.

(7) Tielrooij, K. J.; Song, J. C. W.; Jensen, S. A.; Centeno, A.; Pesquera, A.; Elorza, A. Z.; Bonn, M.; Levitov, L. S.; Koppens, F. H. L. *Nat. Phys.* **2013**, *9*, 248−252.

(8) Fong, K. C.; Wollman, E.; Ravi, R.; Chen, W.; Clerk, A. A.; Shaw, M. D.; Leduc, H. G.; Schwab, K. C. arXiv: 1308.2265, 2013.

(9) Saito, K.; Nakamura, J.; Natori, A. *Phys. Rev. B* **2007**, *76*, 115409.

(10) Muller, M.; Fritz, L.; Sachdev, S. *Phys. Rev. B* **2008**, *78*, 115406.

(11) Foster, M. S.; Aleiner, I. L. *Phys. Rev. B* **2009**, *79*, 085415.

(12) Bolotin, K. I.; Sikes, K. J.; Jiang, Z.; Klima, M.; Fudenberg, G.; Hone, J.; Kim, P.; Stormer, H. L. *Solid State Commun.* **2008**, *146*, 351.

(13) Dean, C. R.; Young, A. F.; Meric, I.; Lee, C.; Wang, L.; Sorgenfrei, S.; Watanabe, K.; Taniguchi, T.; Kim, P.; Shepard, K. L.; Hone, J. *Nat. Nanotechnol.* **2010**, *5*, 722.

(14) Castro, E. V.; Ochoa, H.; Katsnelson, M. I.; Gorbachev, R. V.; Elias, D. C.; Novoselov, K. S.; Geim, A. K.; Guinea, F. *Phys. Rev. Lett.* **2010**, *105*, 266601.

(15) Heinze, S.; Tersoff, J.; Martel, R.; Derycke, V.; Appenzeller, J.; Avouris, P. *Phys. Rev. Lett.* **2002**, *89*, 106801.

(16) Giovannetti, G.; Khomyakov, P. A.; Brocks, G.; Karpan, V. M.; van den Brink, J.; Kelly, P. J. *Phys. Rev. Lett.* **2008**, *101*, 026803.

(17) Ifuku, R.; Nagashio, K.; Nishimura, T.; Toriumi, A. arXiv: 1307.0690, 2013.

(18) Dorgan, V. E.; Bae, M. H.; Pop, E. *Appl. Phys. Lett.* **2010**, *97*, 082112.

(19) Koh, Y. K.; Bae, M. H.; Cahill, D. G.; Pop, E. *Nano Lett.* **2010**, *10*, 4363.

(20) Dorgan, V. E.; Behnam, A.; Conley, H. J.; Bolotin, K. I.; Pop, E. *Nano Lett.* **2013**, *13*, 4581.

(21) As showed in Figure 2a-inset, the $I−V_B$ characteristics at very low V_B are precisely linear (no Joule heating). In which case $V_B/I = dV_B/dI$, and we use the slope to extract R to avoid an error due to a very small (experimental) offset in V_B (few 10 s of micro-Volt). At higher bias, this small offset is negligible and we can safely use $R = V_B/I$. In Figure 2c, T_e is not constant versus V_B due to Joule heating, thus dV_B/dI also contains information about how quickly the temperature is changing with V_B, rather than only the temperature at one specific V_B value. Since (ΔT) is small, we find no significant quantitative difference in our results using either dV_B/dI or V_B/I to extract T_e, but the correct quantity that represents T_e is V_B/I.

(22) Du, X.; Skachko, I.; Barker, A.; Andrei, E. Y. *Nat. Nanotechnol.* **2008**, *3*, 491−495.

(23) Das Sarma, S.; Adam, S.; Hwang, E. H.; Rossi, E. *Rev. Mod. Phys.* **2011**, *83*, 407.

(24) Li, Q.; Das Sarma, S. *Phys. Rev. B* **2013**, *87*, 085406.

(25) Using $n_{tot}(T)$ (Supporting Information Section 3),[6,18] we define an effective chemical potential $\mu_{eff}(T) = \hbar v_F [\pi n_{tot}(T)]^{1/2}$. For instance, for Sample A at $V_G = −5.3$ V and $T = 100$ K, $\mu_{eff}(100$ K$) = 49$ meV. The various V_B necessary to achieve $\Delta T \leq 10$ K in Figure 3 are always significantly smaller than $\mu_{eff}(T)$ and are never larger than 27 mV. We only observe a change in the extracted K_e values (in the doped-regime) when ΔT exceeds 20 K, and $V_B > \mu_{eff}(T)$.

(26) Zuev, Y. M.; Chang, W.; Kim, P. *Phys. Rev. Lett.* **2009**, *102*, 096807.

(27) Hwang, E. H.; Rossi, E.; Das Sarma, S. *Phys. Rev. B* **2009**, *80*, 081413.

(28) Bian, Z.; Zebarjadi, M.; Singh, R.; Ezzahri, Y.; Shakouri, A.; Zeng, G.; Bahk, J. H.; Bowers, J. E.; Zide, J. M. O.; Gossard, A. C. *Phys. Rev. B* **2007**, *76*, 205311.

(29) Minnich, A. J.; Dresselhaus, M. S.; Ren, Z. F.; Chen, G. *Energy Environ. Sci.* **2009**, *2*, 466.

(30) Balandin, A. A. *Nat. Mater.* **2011**, *10*, 569.

(31) Pop, E.; Varshney, V.; Roy, A. K. *MRS Bull.* **2012**, *37*, 1273.